

Numerical studies of cusp formation at fluid interfaces in Stokes flow

By C. POZRIKIDIS

Department of Applied Mechanics and Engineering Sciences, University of California,
San Diego, La Jolla, CA 92093-0411, USA
e-mail: costas@ames.ucsd.edu

(Received 3 June 1997 and in revised form 24 September 1997)

Numerical studies are performed addressing the development of regions of high curvature and the spontaneous occurrence of cusped interfacial shapes in two-dimensional and axisymmetric Stokes flow. In the numerical simulations, the velocity field is computed using a boundary-integral method, and the evolution of the concentration of an insoluble surfactant over an evolving interface is computed using an implicit finite-volume method. Three configurations are considered in detail, and the results are used to elucidate three different aspects of cusp formation. In the first series, the deformation of a two-dimensional bubble immersed in a family of straining flows devised by Antanovskii, and of an axisymmetric bubble immersed in an analogous family of flows devised by Sherwood, are examined. The numerical results indicate that highly elongated and cusped two-dimensional shapes, and pointed or cusped axisymmetric shapes, are unstable and should not be expected to occur in practice. In the second series of studies, the role of an insoluble surfactant on the transient deformation of bubbles subject to the Antanovskii or Sherwood flow is investigated. Under certain conditions, the reduced surface tension at the tips raises the local curvature to high values and causes the ejection of a sheet or column of gas by means of tip streaming. In the third series of studies, the coalescence of a polygonal formation of five viscous columns of a fluid placed in an arrangement that differs only slightly from one proposed recently by Richardson is examined. The numerical results confirm Richardson's predictions that transient cusps may occur at a finite time in the presence of surface tension. The underlying physical mechanism is discussed on the basis of reversibility of surface-driven Stokes flow and with reference to the regularity of the motion driven by negative surface tension. Replacing the inviscid ambient gas with a slightly viscous fluid whose viscosity is as low as one hundredth the viscosity of the cylinders suppresses the cusp formation.

1. Introduction

Considerable interest has arisen in recent years in confirming the spontaneous occurrence and in analysing the geometrical structure of singularities at free surfaces or interfaces in steady or unsteady Stokes flow. An overview of flows where interfacial corners and cusps are known, or have been alleged, to occur was presented by Joseph (1992) and more recently by Pozrikidis (1997*b*). Examples include extensional flow past a bubble, flow induced by a shrinking drop or an expanding bubble, flow underneath a free surface driven by the motion of two counter-rotating rollers or by a point source dipole, and the gravity-driven flow of a liquid layer resting on a horizontal, or flowing down an inclined, wall. More recent contributions were made by Richardson (1997)

and Antanovskii (1996) whose work will be discussed in later sections. Betelú, Diez & Gratton (1997) studied the evolution of two-dimensional interfacial ripples due to a straining flow, and offered further evidence for near-cusp formation in unsteady flow. Betelú (1977) addressed a family of problems involving corner and cusp formation using analytical, numerical, and experimental methods.

One particular family of two-dimensional flows where steady cusped interfacial shapes have been shown to occur was introduced by Antanovskii (1994*a, c*). The arrangement includes a two-dimensional inviscid bubble of equivalent radius a centred at the origin of a stagnation-point flow, as depicted in figure 1(*a*). The unperturbed incident velocity field is given by

$$\left. \begin{aligned} u_x^\infty &= \frac{G}{a^2} x(a^2 + 2c_1(x^2 - 3y^2) + c_2(x^2 + 3y^2)), \\ u_y^\infty &= -\frac{G}{a^2} y(a^2 + 2c_1(3x^2 - y^2) + c_2(3x^2 + y^2)), \end{aligned} \right\} \quad (1)$$

where G is the rate of elongation, and c_1 and c_2 are dimensionless constants. Setting c_1 and c_2 equal to zero yields the familiar irrotational orthogonal stagnation-point flow. The velocity field associated with the constant c_1 is irrotational, the pressure is uniform, and the corresponding flow pattern has four lines of symmetry including the x - and y -axes and two axes that are rotated by 45° with respect to them. The velocity field associated with the constant c_2 is rotational, the pressure does vary with position in the flow, and the corresponding flow pattern has two lines of symmetry including the x - and y -axes, as shown in figure 1(*b*). Antanovskii (1996) showed that the flow near the centre of a four-roller mill apparatus, devised by G. I. Taylor to study drop deformation in extensional flow, is described, to leading order, by the right-hand sides of equation (1) with $c_1 = 0$ and $c_2 = (a/l)^2$; l is the half-size of the mill side.

Richardson (1968) predicted, and more recent numerical studies by Pozrikidis (1997*b*) confirmed, that when the interface has constant tension γ , steady interfacial bubbles shapes subject to the irrotational orthogonal stagnation-point flow are possible only when the capillary number $Ca = 2\mu Ga/\gamma$ has a value that is less than the critical threshold 0.609; μ is the viscosity of the ambient fluid. For lower values of Ca , the bubbles have perfectly elliptical shapes; for higher values of Ca , the transient bubble deformation leads to continued elongation.

Antanovskii (1994*a, c*, 1996) extended Richardson's analysis to non-zero values of c_1 and c_2 , and produced graphs of the deformation parameter $D = (L - B)/(L + B)$ and tip curvature versus Ca ; the lengths L and B are defined in figure 1(*a*). A family of curves corresponding to $c_1 = 0$ and several values of c_2 are shown in figure 2(*a*), adapted from figure 4 of Antanovskii (1996) (in Antanovskii's analysis, the constant c_2 is denoted as ϵ). The monotonically rising curves had been presented earlier by Antanovskii (1994*c*). Figure 2(*a*) reveals the existence of two solution branches when the value of c_2 is sufficiently small: one with slightly and moderately deformed bubbles, and the second with significantly elongated bubbles. The two branches join with hysterical loops. Plotting the tip curvature κ as a function of the capillary number reveals an exponential dependence, as shown in figure 2(*b*), similar to that discovered earlier by Jeong & Moffatt (1992) for a different type of flow. In all cases, as Ca is raised, the bubbles develop pointed ends that lead to cusped shapes. Steady, but not necessarily stable, half-bubble shapes at the transition points for $c_2 = 0.00174$ are depicted in the insets of figure 2(*c*), adapted from figures 7 and 8 of Antanovskii (1996).

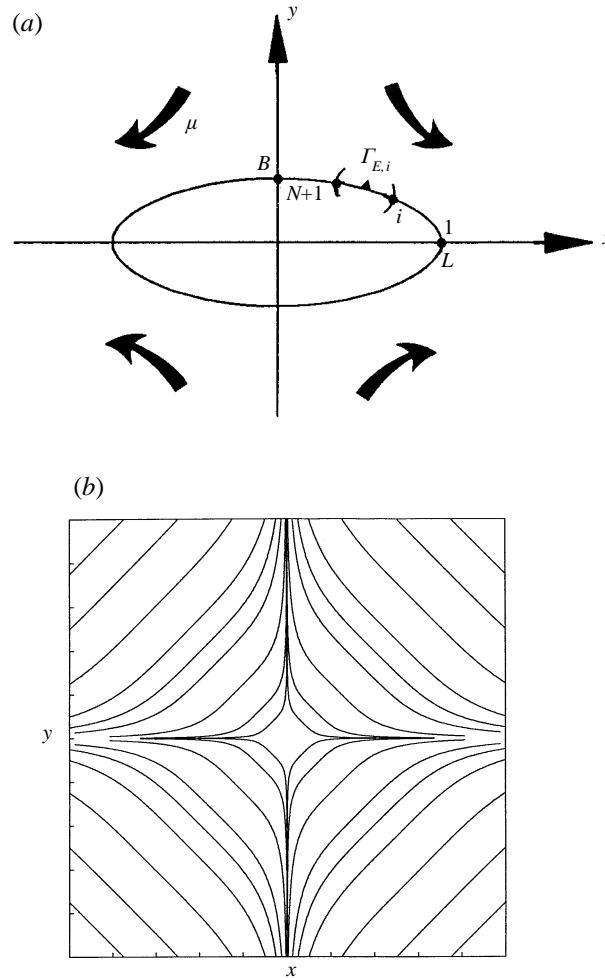


FIGURE 1. (a) Illustration of two-dimensional extensional flow past an inviscid bubble, showing the element discretization. (b) The streamline pattern of the unperturbed flow associated with the constant c_2 that appears in equations (1).

Antanovskii (1996) suggested that the hysterisial loops connect two stable branches, and that sudden transitions between the branches occur at the extremes.

Pozrikidis (1997*b*) attempted, but was unable, to obtain steady cusped shapes as the result of a transient deformation for vanishing surface tension, and suggested that such shapes are unstable. His numerical investigation covered values of c_1 and c_2 in the range where the graph of the function $D(Ca)$ is monotonic. Given this numerical evidence, it appears that the steady shapes are stable only when Ca is less than a critical value that depends on the structure of the incident flow, that is, it depends on the values of c_1 and c_2 . Unfortunately, because of numerical difficulties associated with the large curvature of the interface at the tip, whether this critical value is finite or infinite could not be ascertained.

The recent discovery that two solution branches exist when $c_1 = 0$ and the value of c_2 is sufficiently small, merging to yield a one-to-one function $D(Ca)$ at a certain value of c_2 , as shown in figure 2(c), motivates the re-examination of the stability of the shapes on either side of a hysterisial loop. In the first part of this work, presented in §3, we

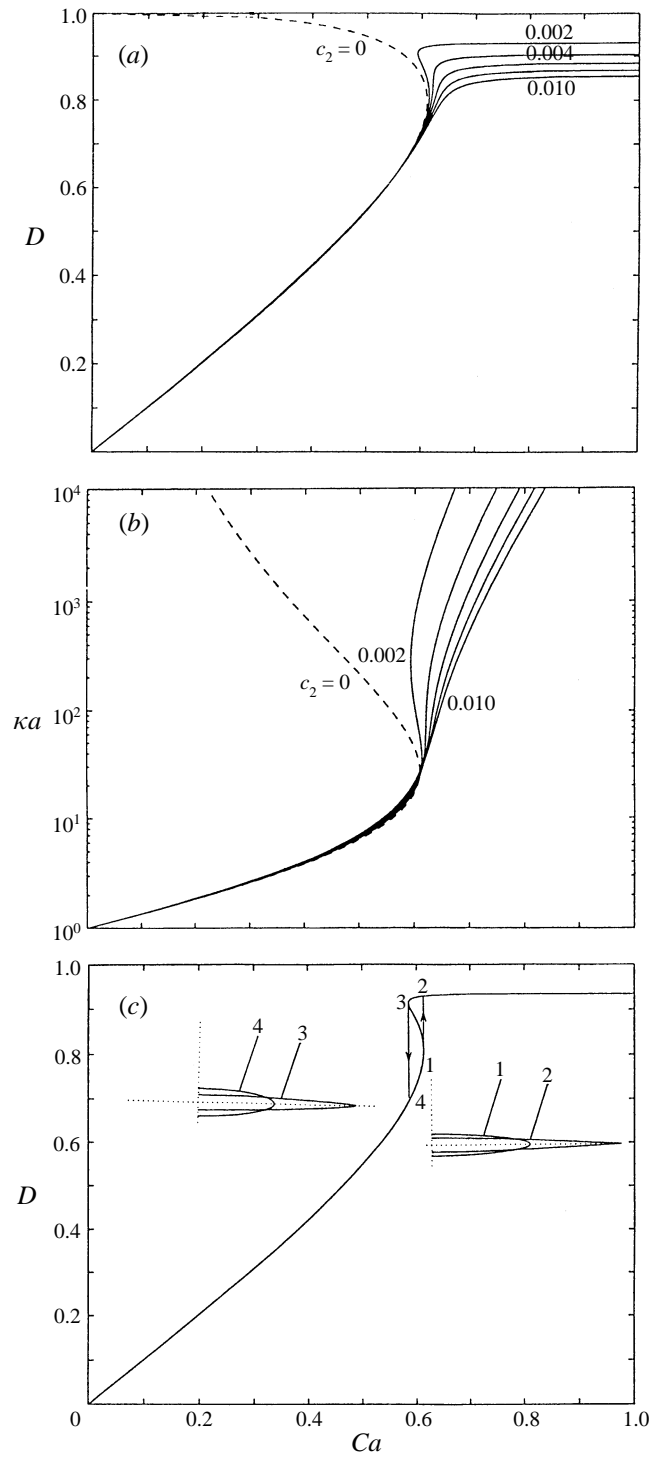


FIGURE 2. For caption see facing page.

offer numerical evidence that the elongated shapes and the cusped shape for zero surface tension are unstable, and thereby cast further doubt on the physical relevance of singular shapes at vanishing surface tension for this particular type of flow.

The two-dimensional flow considered by Antanovskii has an axisymmetric counterpart considered earlier by Sherwood (1984). In cylindrical polar coordinates (x, σ, θ) , the unperturbed incident velocity field is given by

$$u_x^\infty = \frac{G}{a^2} x(a^2 + c_2 x^2), \quad u_\sigma^\infty = -\frac{1}{2} \frac{G}{a^2} \sigma(a^2 + 3c_2 x^2), \quad (2)$$

where a is the equivalent bubble radius and c_2 is a dimensionless constant. Setting $c_2 = 0$ yields the familiar irrotational orthogonal stagnation-point flow with uniform pressure. The velocity field associated with the constant c_2 is rotational, the pressure is non-uniform, and the streamline pattern is topologically similar to that of the orthogonal stagnation-point flow. It is evident that the velocity field (2) is the axisymmetric counterpart of the two-dimensional velocity field (1) with $c_1 = 0$.

Although the correspondence between the Antanovskii and the Sherwood flow has not been recognized explicitly, the behaviours of two-dimensional and axisymmetric bubbles have been compared for the special case of irrotational stagnation-point flow; two-dimensional bubbles are stable only if the capillary number is sufficiently small, as discussed earlier, whereas axisymmetric bubbles appear to be stable for any value of the capillary number, however large. This contrast, however, is softened by the observation that axisymmetric bubbles subject to irrotational stagnation-point flow behave similarly to two-dimensional bubbles subject to the Antanovskii flow for values of c_2 and c_1 that lie in the range where the graph of the function $D(Ca)$ is monotonic. One difference is that, as Ca tends to infinity, the deformation parameter of axisymmetric bubbles tends to unity, whereas that of two-dimensional bubbles tends to a limit that is less than unity.

Using the slender-body approximation which is applicable for elongated shapes, Sherwood (1984) computed families of steady shapes parametrized by the capillary number $Ca^* = c_2^{1/4} \mu G a / \gamma$ and the flow parameter c_2 . His results suggested that when c_2 is zero or positive, steady shapes exist for any value of Ca^* . When $c_2 = 0$, in particular, as Ca^* is raised, the bubble tips tend to obtain conical shapes whose traces in an azimuthal plane form corners; when $c_2 > 0$, as Ca^* is raised, the tips tend to obtain conical shapes whose traces in an azimuthal plane form cusps. Much earlier, Buckmaster (1972) had shown that a true corner may not develop, the slender-body solution is invalid within an exponentially small region near the tips, and the ultimate state of a geometrical singularity is a cusp.

In §3, we present results of numerical simulations on the transient deformation of axisymmetric bubbles subject to the Sherwood flow, and confirm that the formation of cusped shapes is promoted by the nonlinearity of the incident flow. More importantly, we find that, in the absence of surface tension, steady cusped shapes either do not exist, or else are unstable. Consideration of the graphs of the deformation parameter versus the capillary number reveals that the behaviours of axisymmetric and two-dimensional bubbles are not as different as it might have appeared.

FIGURE 2. (a) The deformation parameter D of steady two-dimensional bubbles plotted against the capillary number for an incident flow with $c_1 = 0$ and $c_2 = 0$ (broken line), 0.002, 0.004, 0.006, 0.008 and 0.01. (b) The corresponding bubble tip curvature κ . (c) The deformation curve for $c_2 = 0.00174$; the insets show bubble profiles at the transition points. All figures are reproduced from Antanovskii (1996).

In the second part of this work, we investigate the effect of a surfactant on the deformation and tip curvature of a pointed bubble. The significance of surface tension variations on the transient deformation of a drop subject to an axisymmetric irrotational stagnation-point flow was discussed in detail by Stone & Leal (1990) and Milliken, Stone & Leal (1993). When the viscosity of the drop is equal to that of the ambient fluid, the boundary-integral computations of Milliken *et al.* showed that, depending on the surfactant diffusivity and the sensitivity of the surface tension to the surfactant concentration, a surfactant may act in two different ways: it may either suppress the development of bulbous ends and lead to cigar-like shapes or it may promote the formation of the bulbous ends. For low-viscosity drops, there is strong evidence that the surfactant promotes the formation of spindle-like shapes, but the numerical simulations of Milliken *et al.* were terminated before the tip curvature had reached small values, and tip streaming could not be observed. De Bruijn (1993) reported laboratory observations confirming that a surfactant facilitates tip streaming from a drop that is suspended in a simple shear flow, but a quantitative description was not given. Antanovskii (1994*b*) studied the flow induced by a pair of counter-rotating point vortices underneath a free surface, and confirmed that surfactants facilitate cusp formation. Numerical difficulties prevented the resolution of the local structure of the interface near the cusp.

In §4 of this paper, we study the effect of a surfactant on the transient deformation of a two-dimensional bubble subject to the Antanovskii flow. The main objective is to illustrate in an explicit manner the way in which the accumulation of the surfactant at the tips raises the curvature and causes disintegration. We show that with all other parameters held constant, reducing the surfactant diffusivity may lead to tip streaming, but making the surface tension a more sensitive function of the surfactant concentration may have a mixed influence. A brief consideration of the analogous axisymmetric problem with a bubble suspended in the Sherwood flow reveals similar behaviours.

In the third part of this work, presented in §5, we discuss the formation of transient cusps in unsteady two-dimensional flow driven solely by surface tension. The motivation for undertaking this investigation originates from an important distinction: steady cusps may occur only in the theoretical limit of vanishing surface tension, whereas, at least in principle, transient cusps may occur for any value of the surface tension. Since the curvature at the location of the cusp is infinite, the flow in the neighbourhood of the cusp in the presence of surface tension resembles that due to a two-dimensional point force, and the velocity at the location of the cusp is infinite. The lifetime of the singularity, however, is short enough that the displacement of the interface during the time of cusp formation and disappearance is finite. An exception should be noted: conical interfaces whose traces in an azimuthal plane produce cusped profiles may exist in both steady and unsteady flow. In this case, the flow near this cusp does not resemble that due to a three-dimensional point force and the velocity is finite.

Hopper (1990) suggested that ‘on the basis of the model physics incorporated into the evolution equation, it cannot be possible for a cusp to form in the forward time discretization: Tractions and stresses at the surface would blow up’. While this is a physically understandable viewpoint shared by a number of subsequent authors, the inability of the Stokes equation to spontaneously produce singular behaviours in surface-tension-driven flow has not been argued convincingly by physical reasoning or discounted by analytical methods.

Richardson (1997) studied the coalescence due to surface tension of viscous cylinders in vacuum, and made an astonishing discovery: a transient cusp forms at a critical

condition when a small bubble is about to be trapped within the liquid. His investigation uses a semi-analytical approach based on conformal mapping and on the complex-variable formulation of two-dimensional Stokes flow. In §5 of this paper, we confirm Richardson's predictions, discuss the phenomenon of transient cusp formation with reference to the nature of the reversed flow driven by negative surface tension, and show that replacing the ambient inviscid gas with a slightly viscous fluid suppresses the singular behaviour.

2. Mathematical formulation and numerical method

In subsequent sections, we present the results of numerical simulations on the evolution of a two-dimensional or axisymmetric drop or bubble with viscosity $\mu_2 = \lambda\mu$, placed in an ambient fluid with viscosity μ . We allow the interface to be occupied with an insoluble surfactant whose surface concentration is denoted as Γ . The flow in the exterior or interior of the drop or bubble is governed by the equations of Stokes flow (e.g. Pozrikidis 1997*a*), and the evolution of the surfactant concentration is governed by a convection–diffusion equation discussed in the Appendix. At the initial instant, the surfactant concentration, and thus the surface tension, is uniform over the interface.

For simplicity, we assume that the surface tension γ is related to the surfactant concentration Γ by the linear equation of state

$$\gamma = \gamma_0 \frac{1 - (\Gamma/\Gamma_0)\beta}{1 - \beta}, \quad (3)$$

where the subscript 0 designates the initial value, $\beta = \Gamma_0 RT/\gamma_c$ is a physicochemical constant expressing the sensitivity of the surface tension to the surfactant concentration, R is the ideal gas constant, T is the absolute temperature, and γ_c is the surface tension of a clean interface that is devoid of surfactants. A nonlinear equation of state would have been more appropriate, but it would unnecessarily distract the numerical investigation from its main focus.

The statement of the problem is completed by specifying the initial drop or bubble shape, and by assigning values to the dimensionless property number α and capillary number Ca defined as

$$\alpha \equiv \frac{\alpha\gamma_0}{\mu D_s}, \quad Ca \equiv \frac{\mu G a}{\gamma_0}, \quad (4)$$

where D_s is the surfactant surface diffusivity, and G is a typical rate of elongation of the incident flow. Alternatively, the surfactant surface diffusivity may be expressed in terms of the Péclet number $Pe = Ga^2/D_s = \alpha Ca$. Either of the two dimensionless numbers defined in equations (4) may be replaced by Pe .

2.1. Numerical method

We briefly outline the numerical method for two-dimensional flow; the method for axisymmetric flow arises by straightforward modifications. In the numerical procedure, we trace a quarter of the drop or bubble interface with a collection of $N+1$ marker points, as shown in figure 1(*a*), and describe its shape with blended circular arcs that are subtended across trios of adjacent points. In the presence of surfactant, we assign values of the surfactant concentration to the markers points, denoted as Γ_i , and introduce the average value of the concentration $\Gamma_{E,i}$ over the i th element with end points labelled i and $i+1$, as shown in figure 1(*a*).

The velocity of the fluid at the marker points arises by solving an integral equation of the second kind (e.g. Pozrikidis 1992). In the numerical implementation, the integral equation is converted into a system of linear equations with the unknown vector containing the two components of the velocity at the marker points. The velocity distribution is assumed to vary linearly with respect to arclength between two adjacent marker points. When the viscosity ratio λ has a finite value, including zero, the solution is found by the method of successive substitutions with Gauss–Siedel updating. The eigenfunctions of the double-layer potential corresponding to the dominant eigenvalues are removed to ensure convergence. The number of necessary iterations for a specified relative error of 10^{-6} varies between a few for compact shapes to a few dozen for elongated shapes. When λ is large or infinite, in which case the ambient fluid is nearly or truly inviscid, the linear system is solved by the method of Gauss elimination.

Once the velocity has been computed, the position of the marker points is advanced either with the velocity of the fluid or with the component of the velocity of the fluid normal to the interface. The former is appropriate when a drop or bubble continues to evolve without reaching a steady state, and the latter is appropriate near the steady state.

To update the concentration of the surfactant, we consider equation (A 9) of the Appendix. When the marker points move with the velocity component normal to the interface, we apply the trapezoidal rule to evaluate the two line integrals over the i th interfacial segment, and derive the ordinary differential equation

$$\frac{d\Gamma_{E,i}}{dt} = -\frac{(\Gamma\mathbf{u}\cdot\mathbf{t})_{i+1} - (\Gamma\mathbf{u}\cdot\mathbf{t})_i}{\Delta l_i} - (\Gamma\kappa\mathbf{u}\cdot\mathbf{n})_{E,i} + D_s\left(\frac{\partial\Gamma}{\partial l}\right)_{i+1} - D_s\left(\frac{\partial\Gamma}{\partial l}\right)_i, \quad (5)$$

where Δl_i is the arclength of the i th element. Expressing the nodal values Γ_i on the right-hand side in terms of the element values $\Gamma_{E,i}$, and computing the derivative with respect to arclength at the nodes using second-order differences, we obtain the linear system

$$\begin{aligned} \frac{d\Gamma_{E,i}}{dt} = & -\frac{\alpha_i\Gamma_{E,i+1} + \beta_i\Gamma_{E,i} + \gamma_i\Gamma_{E,i-1} - \Gamma_{E,i}(\kappa\mathbf{u}\cdot\mathbf{n})_{E,i}}{2\Delta l_i} \\ & + D_s(\delta_i\Gamma_{E,i+1} + \epsilon_i\Gamma_{E,i} + \zeta_i\Gamma_{E,i-1}), \end{aligned} \quad (6)$$

where the Greek coefficients are defined in terms of the segments' arclength and tangential velocity. The system of equations (6) was integrated using the implicit Euler method, with all coefficients multiplying the values $\Gamma_{E,i}$ on the right-hand side evaluated at the beginning of the time interval of integration. A similar method was used when the marker points moved with the total velocity of the fluid. This numerical procedure has excellent conservation properties: the total amount of surfactant changed only by a fraction of a percent through the completion of a simulation.

At the initial instant, values of the concentration Γ_i were assigned to the nodes, and the element values $\Gamma_{E,i}$ were computed by the four-point centred interpolation with respect to arclength; the evaluation was done at the middle of each element. Subsequently, the nodal values Γ_i , necessary for the computation of the velocity, arose from the element values $\Gamma_{E,i}$ by an analogous four-point centred interpolation. To resolve regions of high curvature and avoid marker point clustering or dilution, the interface is regridded after each time step using the method described by Pozrikidis (1997*b*). A new feature is the four-point centred interpolation for the surfactant concentration with respect to arclength. Care is taken to preserve the symmetries of the flow in the required interpolations. Regridding and interpolation of the surface

variables are essential for the successful resolution of regions of high curvature. Without them, the numerical investigations would have not been possible.

All computations were executed on a SUN SPARCstation 20 computer with 64 Mbytes of RAM. A complete case study required between 15 min to 25 h of CPU time, with the number of interfacial marker points, ranging between 48 and 500 being the determining factor. The computer code was validated by running numerous tests and confirming agreement with published results, including those presented by Milliken *et al.* (1993) for the deformation parameter of an axisymmetric bubble in the presence of surfactants at steady state.

3. Pointed bubbles with constant surface tension

First, we consider the deformation of a two-dimensional bubble placed in the extensional flow described by equations (1), where $c_1 = 0$ and c_2 has a prescribed value. Antanovskii (1996) presented steady bubble profiles, deformation plots, and tip-curvature graphs for $c_2 = 0.01$. To illustrate the performance of the numerical method, we begin the discussion by comparing our numerical results with Antanovskii's predictions.

At the upper part of figure 3(a), we display steady shapes for $Ca = 0.4, 0.5$ and 0.6 , and a nearly steady shape for $Ca = 0.7$, and compare them with the corresponding shapes displayed by Antanovskii (1996), shown in the lower part. Numerical difficulties prevented us from continuing the computation for $Ca = 0.7$ to longer times, but the increasing magnitude of the curvature at the tip, equal to $50/a$ at the end of the computation, indicated that the interface tends to a steady shape. Antanovskii predicts that the tip curvature of the steady shape is close to $500/a$, which is beyond the capabilities of the numerical method.

In the first three cases, for $Ca = 0.4, 0.5$ and 0.6 , the values of the deformation parameter at steady state, $D = 0.42, 0.54$ and 0.72 , and the normalized tip curvature $\kappa a = 3.9, 6.5$ and 20 , are in excellent agreement with the values read off figures 4 and 5 of Antanovskii (1996). A disagreement occurs in the absence of surface tension, for $Ca = \infty$. The transient shapes shown in figure 3(b), starting from an elongated and a circular shape, do not lead to steady shapes with cusped tips: the bubble continues to elongate. These results are consistent with those reported in our previous study (Pozrikidis 1997b) for $c_2 = 0.05$, and their inclusion in the present work serves only to affirm these earlier predictions.

To illuminate the role of the structure of the incident flow in the evolution of bubbles when the surface tension vanishes, in figure 4 we present typical stages in the evolution of a bubble for $c_1 = 0$ and $c_2 = 0, 0.02, 0.05$ and 0.10 . In all cases, as the bubble begins deforming from the circular shape, the tip curvature increases; but then, as the bubble obtains an elongated shape, the curvature reaches a maximum and starts decreasing. At long times, the bubbles develop two symmetric necks and the interfaces form dimples. Increasing the component of the incident flow associated with the constant c_2 reduces the x -coordinate of the centres of the necks and promotes the formation of the necks. Evidence that a steady cusped configuration arises as the result of the transient motion could not be found.

Next, we consider an incident flow with $c_1 = 0, c_2 = 0.00174$. The dependence of the deformation parameter on the capillary number for steady shapes is illustrated in figure 2(c), after Antanovskii (1996). There is a triplicity of solutions when the capillary number is located within the window (0.585, 0.613). Antanovskii suggested that the upper and lower solution branches are stable, and that sudden transitions occur on the

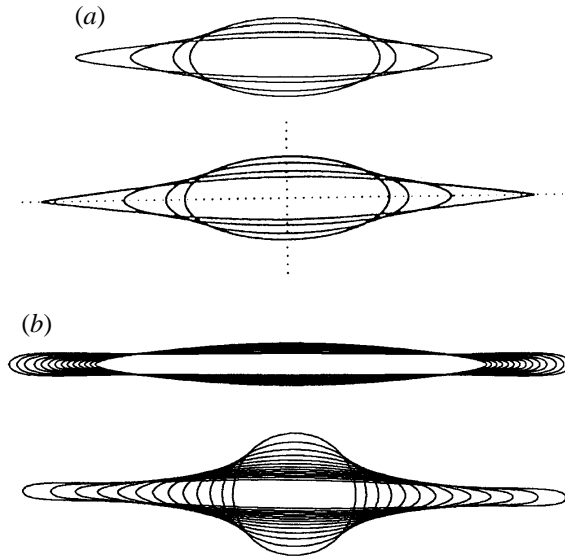


FIGURE 3. (a) The upper part shows computed steady shapes of two-dimensional bubbles for $c_1 = 0$, $c_2 = 0.1$, and $Ca = 0.4, 0.5$ and 0.6 , and a nearly steady shape for $Ca = 0.7$; the lower part shows the corresponding steady shapes presented by Antanovskii (1996). (b) Transient shapes for $Ca = \infty$, starting from an elongated and from a circular shape.

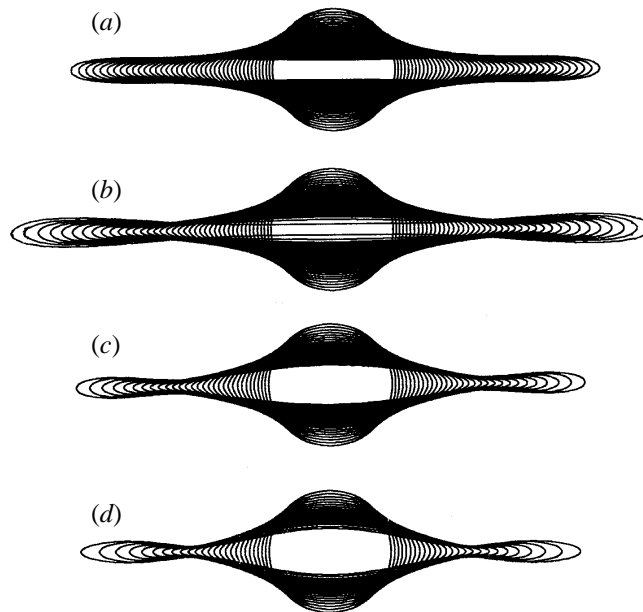


FIGURE 4. Evolving profiles of two-dimensional bubbles for $Ca = \infty$, subject to the incident flow described by equations (1) with $c_1 = 0$, and $c_2 = 0, 0.02, 0.05$ and 0.10 (a–d).

sides of the hysteretical loop as the capillary number approaches the critical value 0.613 from lower values, and similarly for the critical value 0.585 . In contrast, our computations indicate that the lower branch on the left of the point labelled 1 is stable, whereas the upper branch is unstable.

In figure 5(a), we present computed steady bubble shapes for $Ca = 0.60, 0.61$ and 0.61255 , resulting from the transient deformation from the circular initial state. In all

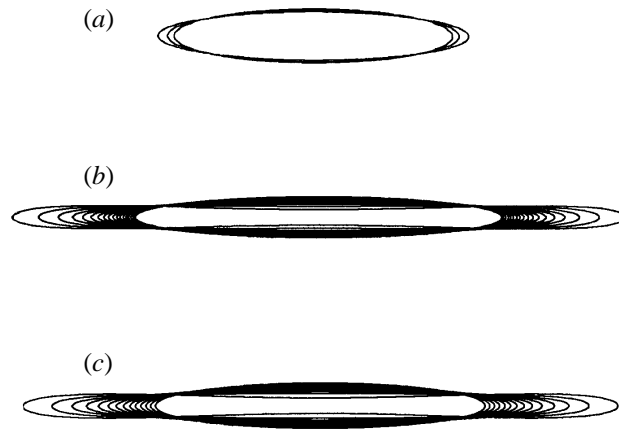


FIGURE 5. (a) Steady bubble profiles resulting from the transient deformation of the circular shape for $c_1 = 0$, $c_2 = 0.00174$ and $Ca = 0.60, 0.61$ and 0.61255 . (b, c) Evolutions that do not lead to steady shapes, for $Ca = 0.61255$ and 0.65 , respectively.

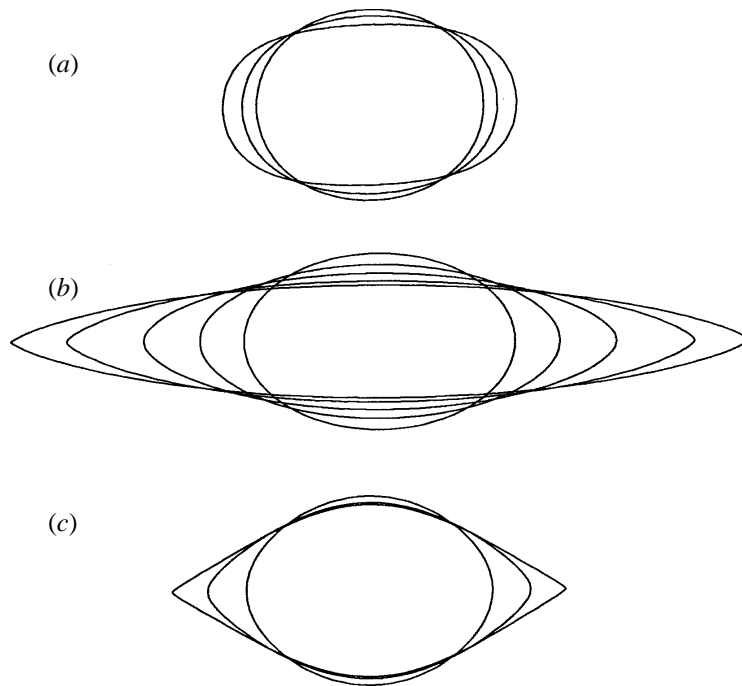


FIGURE 6. Profiles of steady axisymmetric bubbles subject to the Sherwood straining flow; the incident velocity field is given by equations (2). (a) $c_2 = -0.2$ and $Ca = 0.03, 0.06$ and 0.10 ; (b) $c_2 = 0$ and $Ca = 0.06, 0.1, 0.13636\dots, 0.185, 0.227$; (c) $c_2 = 0.5$ and $Ca = 0.03, 0.06$ and 0.1 .

three cases, the deformation parameter at state steady is in excellent agreement with that read off the lower branch of the graph in figure 2(c). Antanovskii suggests that a sudden transition to an elongated shape occurs at $Ca = 0.613$. In figure 5(b, c), we present two evolutions that do not lead to steady shapes, for $Ca = 0.61255$ and 0.65 , beginning with elongated shapes. It appears that, when $Ca = 0.61255$, a steady shape can be reached only from a limited number of initial configurations. Antanovskii's analysis shows the existence of a unique steady shape when $Ca = 0.65$, which, however,

could not be reproduced in our simulations. These results indicate that the highly elongated shapes and the cusped shapes for vanishing surface tension are unstable and should not be expected to occur in the present family of two-dimensional extensional flows.

Next, we consider the deformation of axisymmetric bubbles subject to the extensional flow described by equations (2). Steady bubble shapes arising from the evolution of spherical bubbles for $c_2 = -0.2, 0$ and 0.5 , and for several values of the capillary number $Ca = \mu Ga/\gamma$, are shown in figure 6(a–c). For $c_2 = 0$, the results are in excellent agreement with those presented by Youngren & Acrivos (1976), which is rather surprising. These authors used only 14 interfacial marker points, compared to the over 80 points used in the present work. Youngren & Acrivos computed steady interfacial shapes using an iterative method that circumvents the time-consuming time stepping. The profiles presented in figure 6(c) for $c_2 = 0.5$ show that as c_2 is raised, the bubble tips tend to become increasingly pointed, and cuspidal shapes emerge as predicted by Sherwood (1984) on the basis of the slender-body theory. Increasing c_2 for axisymmetric flow has an effect that is analogous to that of increasing c_2 for two-dimensional flow, in the sense that cusp formation is facilitated in both cases.

In figure 7(a–c), we present stages in the evolution of a spherical bubble for $c_2 = -0.20, 0$ and 0.5 ; in the first case for $Ca = 0.15$, and in the second and third cases in the absence of surface tension, for $Ca = \infty$. When $c_2 = -0.20$, the transient profiles transform into dumb-bells and the interface is a biconcave disk; when $c_2 = 0$, the profiles are nearly elliptical; and when $c_2 = 0.5$, they have spindle-like shapes; a column of gas is ejected from the tips of the bubble along the centreline. The profiles shown in figure 7(c) are qualitatively similar to those photographed by Sherwood (1984) for nearly inviscid drops whose viscosity is 0.01 times that of the ambient fluid. Sherwood's numerical studies of the transient deformation of axisymmetric drops, based on slender-body theory, suggest that when the capillary number is increased beyond a certain level, a thin column of drop fluid is ejected from the tips. The evolving trace of the drop interface in an azimuthal plane is similar to that shown in figure 7(c).

To put the results of the preceding two paragraphs into a unified framework, in figure 8 we plot the deformation parameter at steady state against the capillary number, for four values of c_2 . The high tip curvature prevented us from extending the curves for $c_2 = 0, 0.2$ and 0.5 to larger values of the capillary numbers and higher deformations. The curve for $c_2 = 0$ is in perfect agreement with that presented by Youngren & Acrivos (1976). Remarkably, these authors were able to extend their graph up to $Ca = 0.258$, even though they used a significantly lower number of marker points. The curve for $c_2 = -0.20$ terminates at a critical capillary number beyond which steady shapes could not be obtained, even though the bubble maintained a rounded shape throughout the evolution. This behaviour is in agreement with Sherwood's (1984) discovery that steady solutions, computed using the slender-body theory, break down when the capillary number is raised beyond the value where $(a/L)^2 = -c_2$, where L is the bubble half-length; at that point, the tips are located at stagnation points (this is deduced from statement on p. 284 of Sherwood's article that, in his notation, solutions break down when $G_3^* l^2 = -1$). For $c_2 = -0.20$, the predicted critical bubble length is $L/a = 2.24$ which is in fair agreement with the results of the present numerical computations.

The general similarity between the curves displayed in figure 8 and the bottom-left portions of the curves in figure 2(a) corresponding to values of c_2 around 0.01 makes it tempting to suggest that a hysteresis loop joining two partially overlapping solution

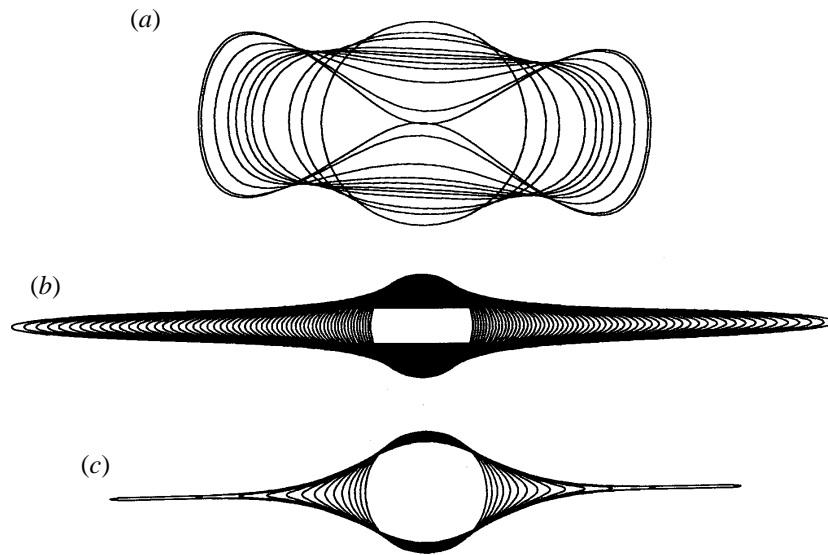


FIGURE 7. Stages in the deformation of axisymmetric bubbles subject to the Sherwood straining flow. (a) $c_2 = -0.2$ and $Ca = 0.15$; (b) $c_2 = 0$ and $Ca = \infty$; (c) $c_2 = 0.5$ and $Ca = \infty$.

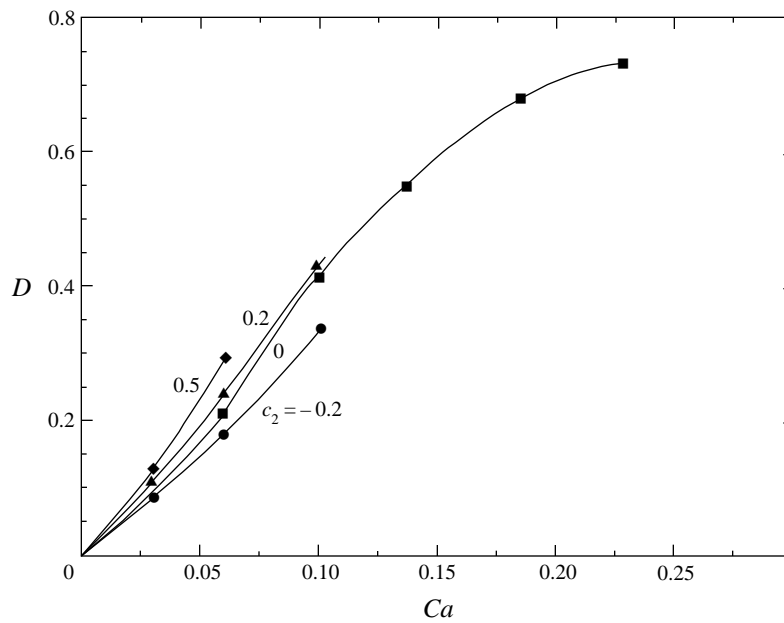


FIGURE 8. Deformation parameter of steady axisymmetric bubbles as a function of the capillary number for several flows with $c_2 = -0.2, 0, 0.2$ and 0.5 . The curve for $c_2 = -0.2$ terminates at a critical capillary number beyond which steady shapes do not arise. The other curves terminate at points where the numerical method was unable to produce highly curved shapes.

branches appears at a critical negative value of c_2 in the case of axisymmetric flow; whether or not this is true must await further analysis. What is now certain is that axisymmetric bubbles subject to the Sherwood flow behave similarly to two-dimensional bubbles subject to the Antanovskii flow, provided that the comparison is made at appropriate values of the parameter c_2 . In both cases, perfectly cusped shapes do not arise.

4. Pointed bubbles with variable surface tension

In this section, we turn to considering the effect of a surfactant on the transient deformation of pointed bubbles. Surfactant non-uniformities cause variations in the surface tension and produce tangential discontinuities in the interfacial stresses identified by Marangoni. The associated fluid motion may have a profound effect on the shape of a drop or bubble, as well as on its ability to withstand the deforming action of an incident flow.

The physical processes by which surfactant transport affects the deformation of an axisymmetric drop or bubble subject to a stagnation-point flow were discussed by Stone & Leal (1990), and more recently by Milliken *et al.* (1993), Pawar & Stebe (1996), and Li & Pozrikidis (1997). Under the influence of the axisymmetric flow, the surfactant is convected from the main body of a drop or bubble towards the tips, and this causes the surface tension to be raised at the waist and be lowered at the tips. At the same time, the increase in the bubble surface area due to the deformation causes a global surfactant dilution, which raises the level of the surface tension. The interplay between surfactant accumulation and dilution determines the net deformation. Our interest lies in investigating the effect of the surfactant on the tip curvature, rather than in quantifying the magnitude of the deformation.

At the outset, we clarify the role of the surfactant diffusivity D_s . At first sight, it might appear that as D_s tends to vanish, while all other dimensionless parameters are held constant, the surfactant will keep being convected from the waist towards the tips, and its accumulation will cause a continuous decrease in the tip surface tension leading to cusp formation or disintegration. This reasoning, however, overlooks the retardation of the interfacial velocity field due to the Marangoni stresses: when a sufficiently strong surfactant and associated surface tension field have been established, the Marangoni motion will oppose the outward motion due to the external flow, and the interface will be immobilized. Thus, lowering the surfactant diffusivity while keeping all other parameters constant does not necessarily lead to disintegration, unless the capillary number is sufficiently high.

To clearly demonstrate this behaviour, in the inset of figure 9(a) we present steady two-dimensional bubble shapes subject to the Antanovskii flow for $c_1 = 0$ and $c_2 = 0.05$, $Ca = 0.40$, $\beta = 0.50$ and $\alpha = 0.10, 5, 50$ and 500 or $Pe = 0.40, 2, 20$ and 200 . In figure 9(a-c) we display the corresponding distributions of the surfactant concentration, surface tension, and tangential velocity, all plotted against normalized arclength. The differences between the flows with $\alpha = 50$ and 500 are small; the effect of the surfactant diffusivity is diminished when α is on the order of 10^2 . Figure 9(c) shows that, as α is raised, the magnitude of the tangential velocity tends to zero uniformly over the interface, and becomes exceedingly small when $\alpha = 500$. In this limit, we encounter Stokes flow past a slender cylinder whose boundary coincides with the bubble interface. Figure 9(b) illustrates the two salient effects of surfactant transport: a global increase in the surface tension due to dilution, and a local decrease at the tips due to surfactant accumulation.

Stone & Leal (1990) showed that increasing the value of the parameter β , that is, making the surface tension a more sensitive function of the surfactant concentration,

FIGURE 9. Steady shapes of two-dimensional bubbles, shown at the inset of panel (a), and the corresponding distributions of (a) surfactant concentration, (b) surface tension, and (c) tangential velocity u_t , plotted against normalized arclength l measured from the mid-plane $x = 0$, where l_0 is the arclength of a quarter of the interface, in a flow with $c_1 = 0$, $c_2 = 0.05$, $Ca = 0.40$, $\beta = 0.50$, and $\alpha = 0.10, 5, 50$ and 500 or $Pe = 0.40, 2, 20$ and 200 .

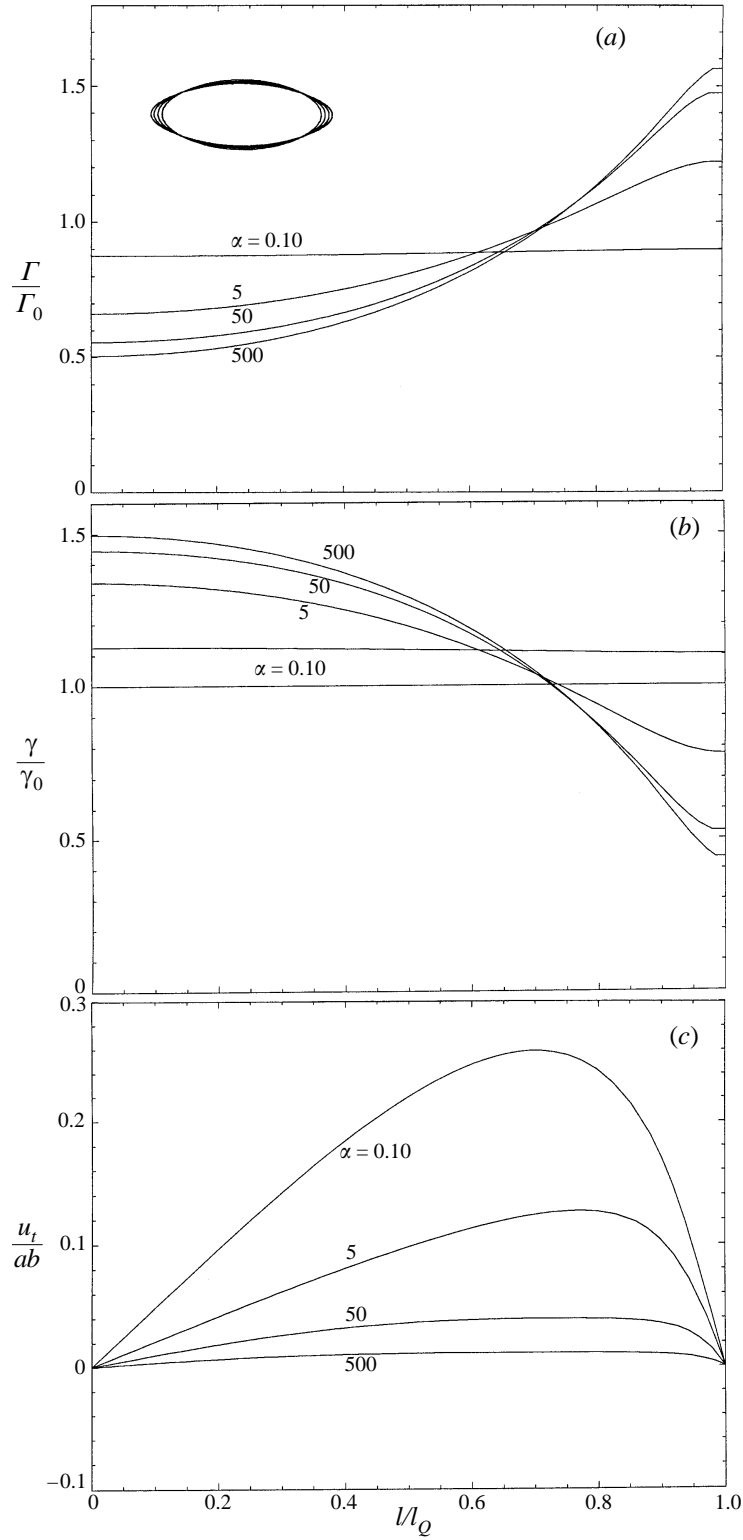


FIGURE 9. For caption see facing page.

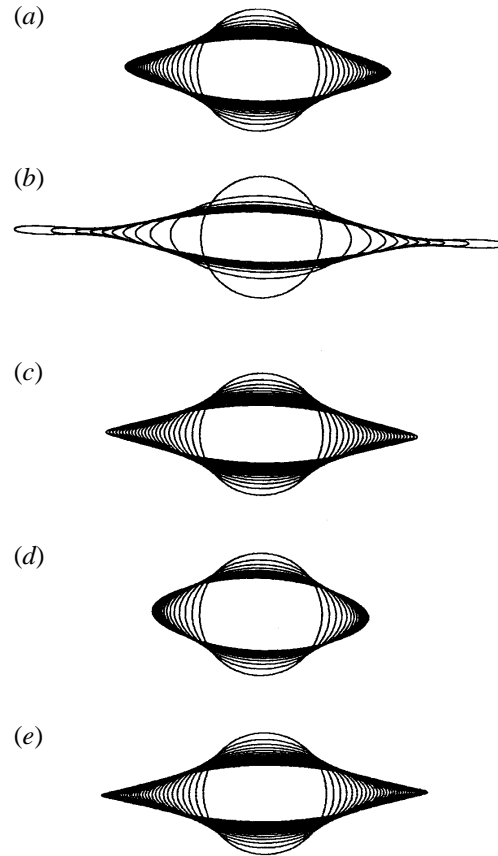


FIGURE 10. Stages in the deformation of two-dimensional bubbles in the presence of surfactants for a flow with $c_1 = 0$, $c_2 = 0.05$, at $Ca = 0.60$, and (a) $\beta = 0$, (b) $\alpha = 50$, $\beta = 0.2$, (c) $\alpha = 50$, $\beta = 0.50$, (d) $\alpha = 50$, $\beta = 0.8$, (e) $\alpha = 500$, $\beta = 0.5$.

while keeping all other parameters constant, does not necessarily lead to disintegration, unless the capillary number is sufficiently large. More will be said about this dependence later in this section.

Next, we consider the behaviour of the bubble when the capillary number is large enough so that the accumulation of the surfactant at the tip has an important effect on the stability of the interface. As a test case, we consider a flow past a two-dimensional bubble with $c_1 = 0$, $c_2 = 0.05$, for $Ca = 0.60$. In figure 10(a–e), we show typical stages in the deformation of bubbles, at evenly spaced time intervals, for $\alpha = 50$ and $\beta = 0$, 0.20, 0.50 and 0.80, and for $\alpha = 500$ and $\beta = 0.5$. In figure 11(b–d), we show the distributions of the surface tension for the last four cases, plotted with respect to reduced arclength; and in figure 12(a, b) we plot the evolutions of the deformation parameter and tip curvature.

For the bubble shown in figure 10(a) corresponding to $\beta = 0$, the surface tension remains constant, equal to the initial value, at all times. Under the prescribed conditions, the bubble tends to a steady shape, as shown in figure 10(a), which is in excellent agreement with that predicted by Antanovskii (1994a). The curvature at the tip also tends to a constant value that is estimated to be close to $28/a$.

Consider now the evolution shown in figure 10(c), corresponding to $\alpha = 50$ and $\beta = 0.50$. The decreased surface tension at the tip causes the tip curvature to be raised

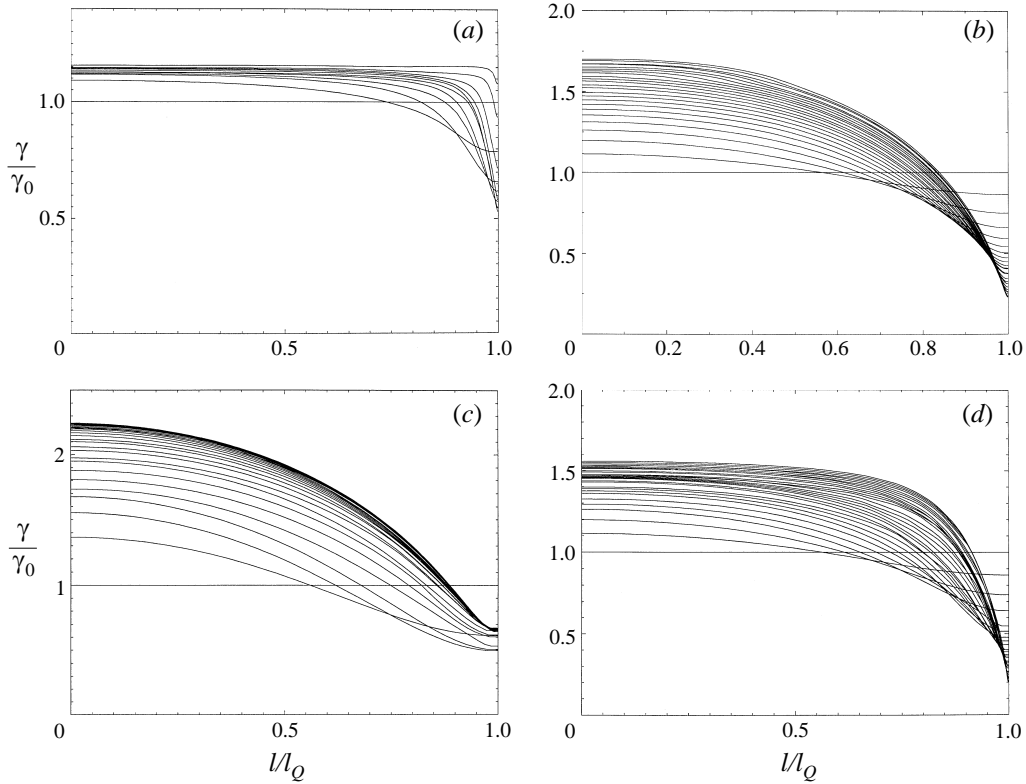


FIGURE 11. Distributions of the surface tension corresponding to the shapes shown in figure 10(b–e). (a) $\alpha = 50$, $\beta = 0.2$, (b) $\alpha = 50$, $\beta = 0.50$, (c) $\alpha = 50$, $\beta = 0.8$, (d) $\alpha = 500$, $\beta = 0.5$.

over time in a monotonic manner to notably high values. As the deformation proceeds, the surface tension over the main body is increased to over 1.5 times the initial value due to surfactant depletion. The motion was followed up to the point where the computations required an exceedingly small time step to prevent numerical instabilities. In spite of this limitation, we have obtained confirmation that the presence of the surfactant causes the bubble tips to become considerably more pointed.

In physical terms, increasing the value of β may be regarded as increasing the total amount of surfactant over the interface, which promotes the drop deformation by lowering the surface tension. But since the surface tension of the clean interface γ_c is related to the initial surface tension γ_0 by $\gamma_c = \gamma_0/(1-\beta)$, if the capillary number defined with respect to γ_0 is kept constant, increasing β also amounts to increasing the surface tension of the clean interface, which restrains the drop deformation. Stone & Leal (1990) showed that for drops that maintain a compact shape, the second effect dominates the first one at any value of α and Ca .

For point bubbles, we observe a somewhat different behaviour. The curves for $\alpha = 50$ and $\beta = 0.20$ and 0.80 shown in figure 12(a) lie below those corresponding to $\beta = 0.50$. In this case, the bubble responds more strongly to the external flow at a value of β that is placed somewhere between 0.20 and 0.80 , probably close to 0.50 . At long times, the deformation parameter for $\beta = 0.20$ increases in a monotonic manner suggesting continuous elongation, whereas that for $\beta = 0.80$ tends to a limit. These behaviours are consistent with the shapes presented in figure 10(b, d). It is interesting to note, in particular, that as the bubble begins deforming, the tip curvature for $\beta =$

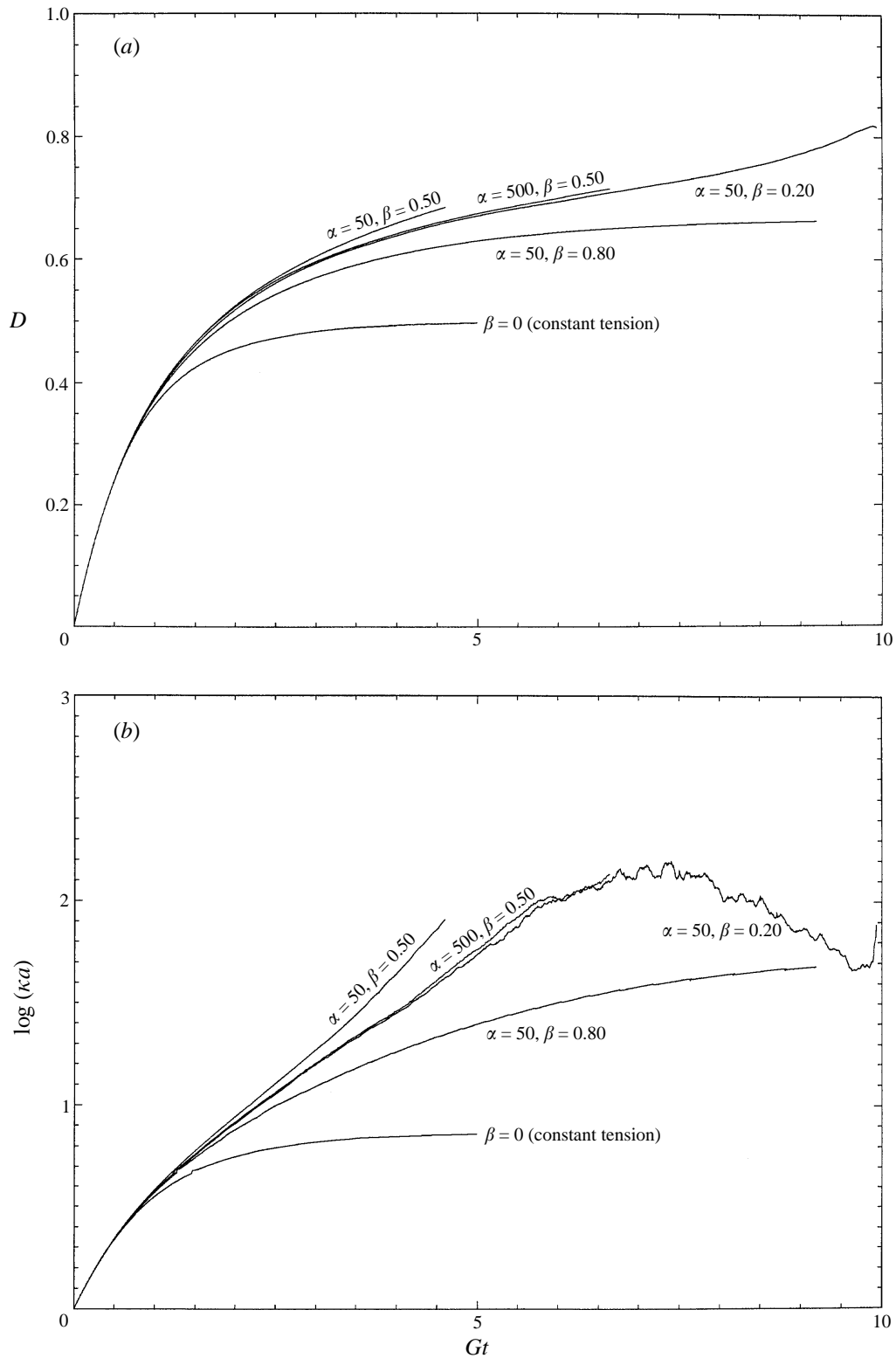


FIGURE 12. Evolutions of (a) the deformation parameter, and (b) the tip curvature κ for $c_1 = 0$, $c_2 = 0.05$, at $Ca = 0.60$ and the indicated values of α and β .

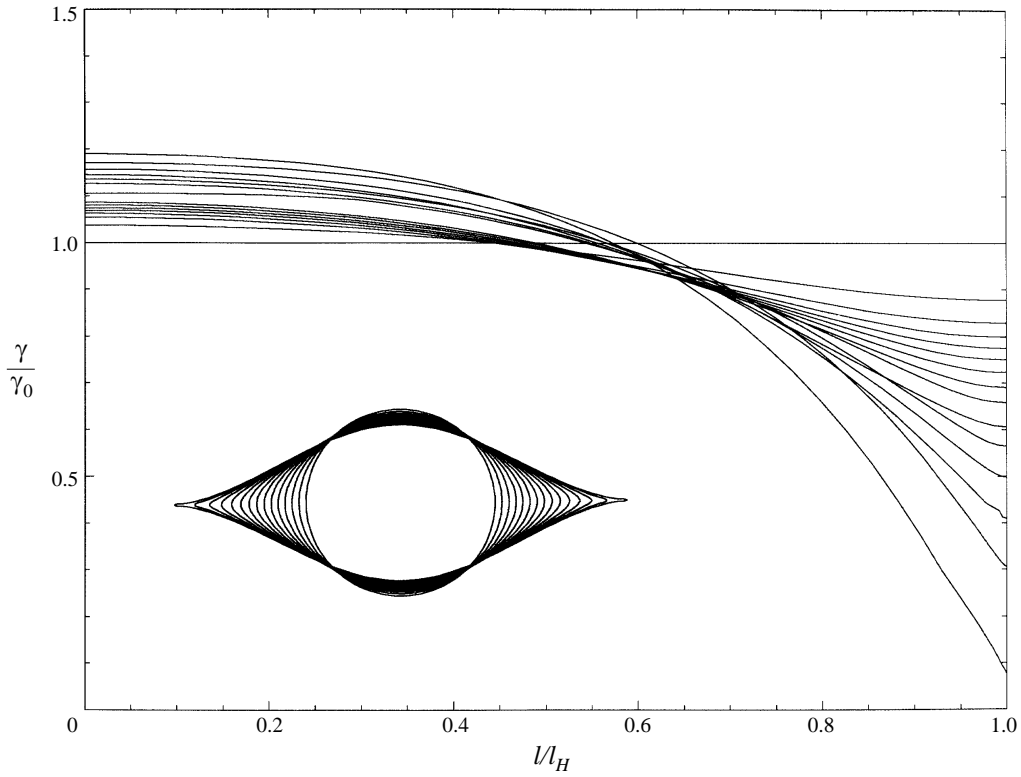


FIGURE 13. The inset shows a sequence of transient profiles of an axisymmetric bubble subject to the Sherwood flow, leading to tip streaming, for $c_2 = 0.50$, $Ca = 0.1$, $\alpha = 1$, and $\beta = 0.5$. The distribution of the surface tension at the corresponding times plotted against normalized arclength l measured from the mid-plane $x = 0$; l_H is the arclength of a half the trace of the interface in an azimuthal plane.

0.20 increases, reaches a maximum, and then it starts decreasing; a thin sheet of gas is extracted from the bubble in the process of tip streaming. Figure 11(a) confirms that, at long times, the surface tension over the main body of the drop tends to that of an uncontaminated interface, given by $\gamma_c = 1.25\gamma_0$.

Figure 10(e) presents stages in the deformation of a bubble with a small surfactant diffusivity corresponding to $\alpha = 500$ and $\beta = 0.50$. Comparing these profiles with those shown in figure 10(c) for $\alpha = 50$ and $\beta = 0.50$, and inspecting the respective distributions of the surface tension and evolution of the deformation parameter and tip curvature, we find noticeable but small differences. For the reasons stated in a previous paragraph, driving the diffusivity to zero does not necessarily lead to tip streaming, unless the value of the parameter β lies within a certain range.

Similar behaviours were observed for axisymmetric bubbles subject to the Sherwood flow, although the computations were more difficult to carry out due to the more pronounced spindle-like shapes. For example, in the inset of figure 13(a), we present a sequence of transient profiles leading to tip streaming for $c_2 = 0.50$, $Ca = 0.1$, $\alpha = 1$ and $\beta = 0.5$. The distribution of the surface tension at the corresponding times is plotted in the main part of this figure. As the surfactant accumulates at the tips, the surface tension decreases dramatically allowing the development of high curvature and tip streaming. If the surface tension were constant, the bubble would deform to a steady shape.

5. Coalescence of five cylinders

Richardson (1997) considered the evolution of an arrangement of liquid columns that allows the study of transient cusps in a two-dimensional flow driven solely by surface tension. In an earlier study, Pozrikidis (1997*b*) was unable to observe cusp formation in a gravity-driven flow in the presence of surface tension, though he confirmed it in the absence of surface tension. Richardson scrutinized the motion near the critical conditions when a bubble is about to be trapped within the liquid whose interface unravels towards an equilibrium position. At sub-critical conditions, the interface evolves without pinching; at super-critical conditions, two non-adjacent sections of the interface touch, entrapping a bubble; at the critical condition, a transient cusp forms.

Physical intuition might suggest that, in the presence of surface tension, an interface will remain smooth at all times. But the argument can be made that the local radius of curvature of a pointed interface is determined by the value of a local capillary number defined with respect to the local magnitude of the velocity of the fluid: the higher the capillary number, the smaller the radius of curvature. Since, due to the increasing magnitude of the velocity during the process of cusp formation the capillary number is driven to infinity, one has to accept the possibility that the local radius of curvature may tend to zero, and a singularity may occur in a spontaneous fashion at a finite time.

In Richardson's model, the fluid resides in the interior of five circles: a central circle of radius a , and four circles of radii b arranged tangentially to the central one and positioned regularly around its perimeter, as shown in figure 14. The non-overlapping of the circles requires that $a/b > \sqrt{2} - 1 = 0.4142\dots$. At the initial instant, the interfaces are broken up at the points of contact, and the five cylinders coalesce to form a larger descendant. This configuration serves as a local model of the flow due to the sintering of long fibres.

In the present numerical investigation, the initial geometry is smoothed out by replacing the cusps with circular arcs whose radii are equal to $0.10a$. The small arcs are tangential to the central cylinder and one of the outer cylinders, as shown in figure 15(*a-c*). The initial distribution of interfacial curvature is discontinuous at the points where the circles touch; in Richardson's configuration, the curvature is infinite at the points of contact. The smoothing of the cusps is not likely to have an important effect on the character of the motion a short time after the beginning of the flow: the analytical solution of Hopper (1990) describing the sintering of two cylinders shows that the cusps disappear immediately yielding infinitely differentiable smooth shapes.

Richardson's (1997) semi-analytical solution in complex variables revealed that when $a/b = 0.575$, a transient cusp forms as the interface is pulling out from the enclosures, as shown in figure 14(*b*); our numerical computations confirm this prediction, but with a different critical ratio a/b due to differences in the initial shape. In figure 15(*a-c*), we present a sequence of transient profiles for $a/b = 1$, 0.675 and 0.575, which are analogous to those shown in figure 14(*a-c*), and observe that a nearly cusped shape tends to form when $a/b = 0.675$. The computation was stopped when the interfacial curvature became so large that the fine details of the motion could not be resolved with adequate accuracy. In figure 16, we illustrate the evolution of the curvature and radial velocity at the point where the interface meets the horizontal axis for $a/b = 0.675$, and observe evidence that both tend to become singular at a finite time. It would be illuminating to analyse the physics of the motion near the time of cusp formation, and to probe the temporal dependence of the cusp curvature and

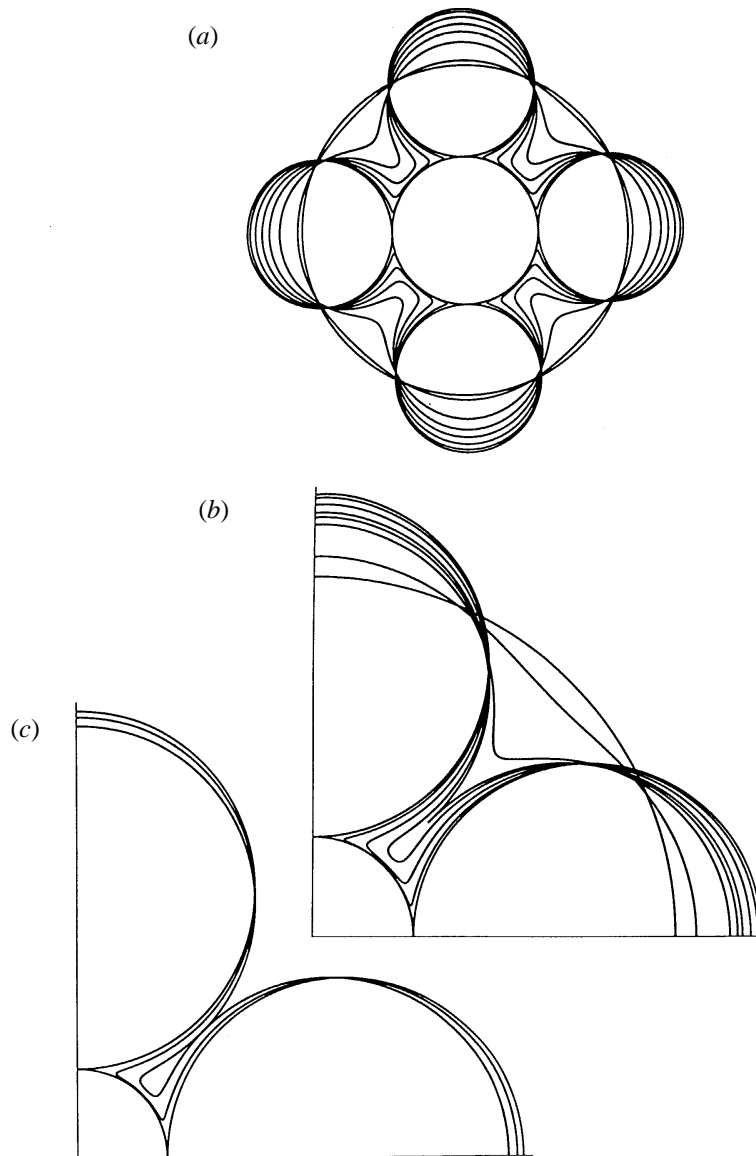


FIGURE 14. Stages in the coalescence of five cylinders in vacuum, driven by surface tension, after Richardson (1997); a is the radius of the central cylinder, and b is the radius of the peripheral cylinders. (a) $a/b = 1.0$, (b) $a/b = 0.575\dots$, (c) $a/b = 0.5$. Only one quarter of the interfaces are shown in (b, c).

velocity, but the numerical results are not sufficiently accurate for that purpose. Richardson's semi-analytical approach is better suited to study the local behaviour.

Two features of the motion are worth emphasizing. First, it is evident from figures 14 and 15 that as the high-curvature points move along the perimeter of the central cylinder, the outer cylinders open up like elastic shells with little distortion. Second, in the numerical computations, we exploited the symmetry of the flow with respect to the horizontal and vertical axes, but not the symmetry with respect to the diagonal axes. We found that a slight asymmetry in the marker point distribution with respect to the diagonal axes causes the peripheral circles to tilt towards the left or right, closing one

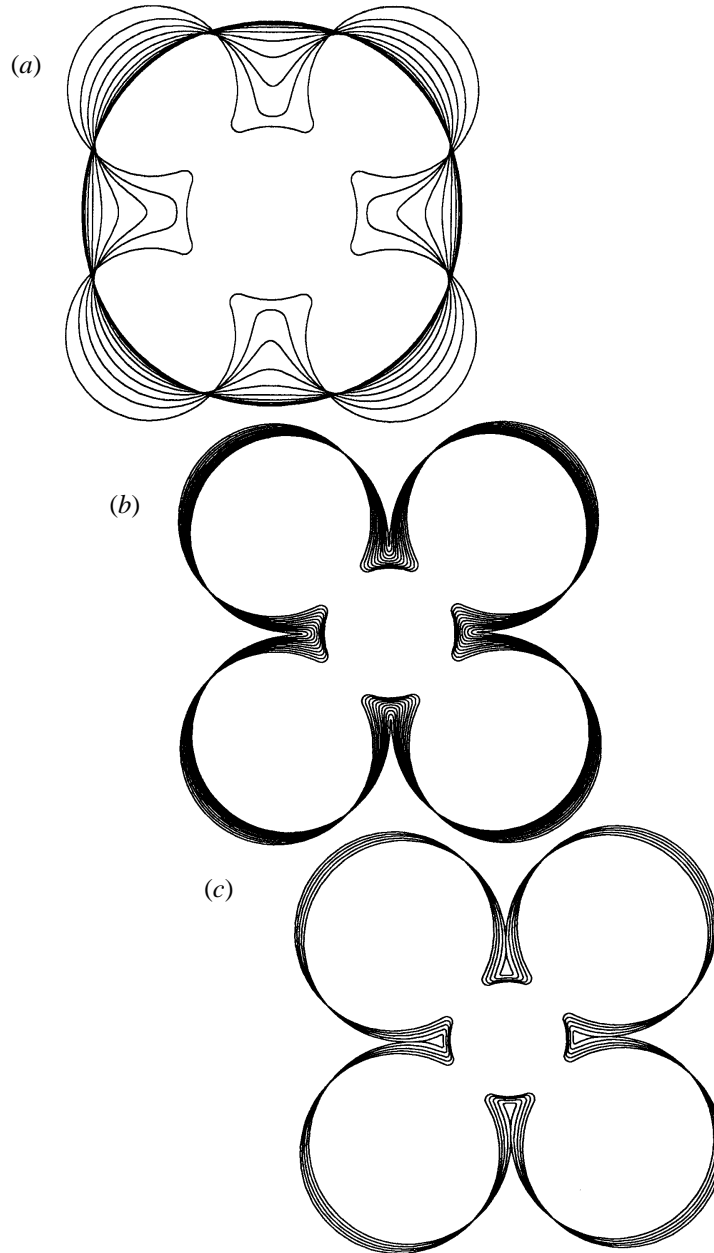


FIGURE 15. Coalescence of five cylinders in vacuum, computed by the boundary-integral method, for (a) $a/b = 1.0$, (b) $a/b = 0.675$ and (c) $a/b = 0.575$.

gap and opening another. This asymmetry, however, did not prevent a cusp from forming on one side. An experimentalist who wishes to study cusp formation in the laboratory should be aware of this unstable behaviour.

The first of the aforementioned features motivates the investigation of the effect of the viscosity on the ambient fluid. In vacuum, nothing prevents opposing sections of the interfaces from deforming like elastic shells or from touching and developing cusps. But if the ambient fluid is viscous, its drainage from the narrow gaps will delay, but not

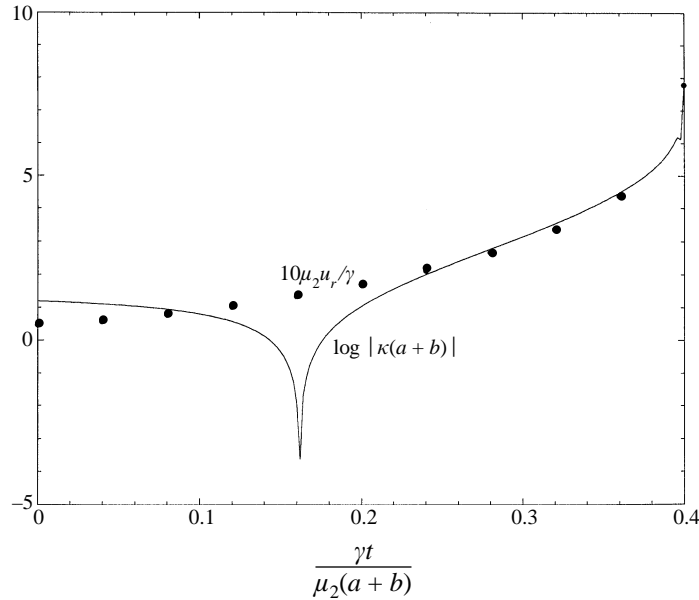


FIGURE 16. Evolution of the curvature κ and radial velocity u_r at the point where the interface meets the horizontal axis for $a/b = 0.675$. Solid line shows the curvature, circles show the velocity.

necessarily prevent, the touching of the interfaces, and is likely to suppress the formation of cusps. To investigate this possibility, we replaced the external inviscid medium with a viscous fluid of viscosity μ , where $\mu_2 = \lambda\mu$ is the viscosity of the fluid occupying the cylinders. The evolutions shown in figures 14 and 15 correspond to $\lambda = \infty$. The value $\lambda = 0$ corresponds to five inviscid bubbles coalescing in an ambient liquid under constant volume.

The coalescence of cylinders with $a/b = 1$ and $\lambda = 100$ is virtually indistinguishable from that shown in figure 15(a) for $\lambda = \infty$. In figure 17(a–c), we present sequences of evolving shapes for nearly touching initial shapes with $a/b = 0.42$, for $\lambda = 0.1, 1$ and 100. In the first two cases, transient bubbles of ambient fluid form within the narrow gaps as the interfaces unfold. The necks supporting the bubbles are thicker than the minimum interfacial separations down the crevices at the initial instant, and opposite sections of the interfaces do not touch. As λ is raised, and the ambient fluid becomes less viscous, the bubbles become less rounded and more elongated; for $\lambda = 100$, they transform into strips. The details of the evolution for $\lambda = 100$ shown in figure 17(c) differ significantly from those shown in figure 15(b, c) for $\lambda = \infty$, which is rather surprising. In figure 15(b, c), we observe that, as the outer circular interfaces open up, the sides of the peripheral cylinders move against each other, which is in contrast with the motion shown in figure 17(c).

In figure 17(d), we plot the evolution of the interfacial curvature at the points where the interfaces cross the horizontal axis. For $\lambda = 100$, we note a pronounced maximum in the magnitude of the curvature at some point during the evolution. Unfortunately, owing to numerical difficulties associated with the numerical solution of the linear system emerging from the boundary-integral equation, reliable results for tighter-spaced cylinders and for values of λ higher than a few hundred could not be obtained. It is nevertheless certain that a value of λ much higher than a few hundred is required for a singular behaviour. Thus, a slightly viscous external fluid radically alters the character of the motion within the gap, to the point of suppressing cusp formation.

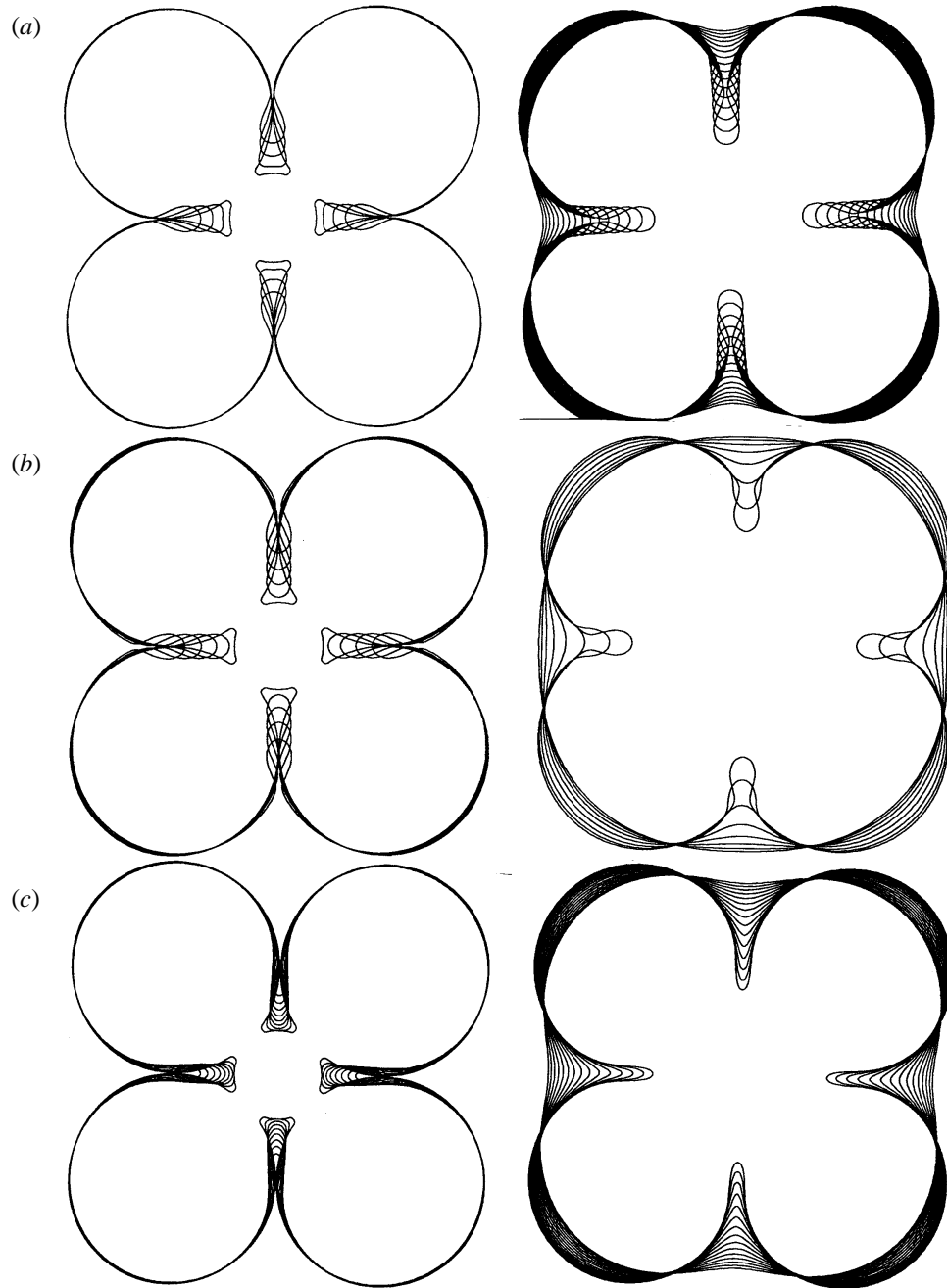


FIGURE 17. For caption see facing page.

The phenomenon of transient cusp formation in a surface-tension-driven flow is intriguing both from a physical and a mathematical standpoint. A cusped interfacial shape may certainly be prescribed in the initial condition of a problem, no matter what the value of the surface tension. Hopper (1990) showed that the interface will evolve at an infinitely fast rate so as to obtain a perfectly smooth shape. Now, reversibility of surface-tension-driven Stokes requires a one-to-one correspondence between the initial

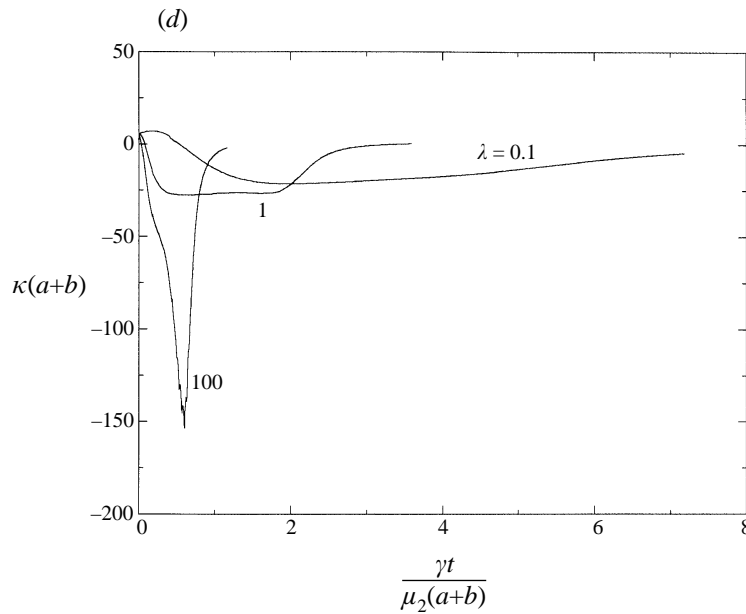


FIGURE 17. Sequences of evolving shapes for nearly touching initial shapes with $a/b = 0.42$, for (a) $\lambda = 0.1$, (b) 1 and (c) 100. The frames on the right are continuations of those on the left, separated for visual clarity. (d) The corresponding evolution of the interfacial curvature κ at the point where the interface crosses the horizontal axis.

cusped and the continuous family of transient evolving smooth shapes, and this can be used to ascertain the character of the fluid motion driven by negative surface tension, and to offer a reason for the formation of transient cusps.

Consider, as an example, the coalescence of two initially tangential viscous circular cylinders. Asymptotically at long times, the motion will lead to a larger circular cylinder whose area is equal to the sum of the areas of the ancestral cylinders. The asymptotic shape of the interface at long but finite times is nearly circular, but enough geometrical information is retained through the evolution so that when the sign of either time or surface tension is reversed, the interface evolves back to the initial cusped shape. That negative surface tension may lead to a cusped shape is not surprising, but what is perhaps unexpected is that the exponentially decaying deviation of the interface from the asymptotic circular shape carries enough information on the precise geometry of the interface at the initial instant. Since two slightly different asymptotic shapes may correspond to vastly different initial shapes, the problem of interfacial evolution with negative surface tension is classified as ill-posed.

Under the influence of negative surface tension, a mass of fluid will be broken up into smaller disjointed pieces in an effort to raise the interfacial area under the constraint of constant volume. The breakup must necessarily occur through the formation of transient cusps, no matter what the viscosities of the fluids. The sequences of shapes shown in figure 14(b) suggest that, when the surface tension is negative, a properly perturbed nearly circular interface will spontaneously form cusps in an attempt to divide, and will then proceed to pinch itself once more thus separating into five cylinders. The first pinching may be regarded an unsuccessful attempt to divide. The only truly unexpected consequence of cusp formation in the presence of surface tension is then that the velocity at a point in the fluid becomes infinite at a finite time, and the reason for this singular behaviour is attributed solely to the flow.

The counterpart of Richardson's arrangement in three dimensions is a composition of spheres: a central one of radius a , and several others of radii b placed tangentially to it. When b/a is sufficiently large, it is possible that opposing sections of the interfaces of the satellite spheres will touch and coalesce at a *point*, at some time during the sintering. When b/a is small, the interfaces will unravel towards the equilibrium spherical shape without touching. At the threshold between these two behaviours, we obtain an interface with a cusped three-dimensional shape. In general, the surface integral of the mean curvature over an infinitesimal area containing the cusp will not be finite, and the flow near this cusp will not be similar to that due to a three-dimensional point force, although circumstances where this may occur may arise.

Dr Steve Yon contributed to the development and implementation of the finite-volume method for the surfactant transport. Professor Stanley Richardson provided me with a preprint of his work that motivated the numerical investigation presented in §5. Support for this work was provided by the National Science Foundation, and the SUN Microsystems Corporation. Acknowledgement is made to the Donors of the Petroleum Research Fund, administered by the American Chemical Society, for partial support of this research.

Appendix. Evolution equations for the surfactant concentration, and finite-volume formulation

In this Appendix, we present the Cartesian form of the convection–diffusion equation governing the change in the concentration of a surfactant at the position of marker points distributed over an evolving three-dimensional, axisymmetric, or two-dimensional interface. In addition, we introduce a finite-volume formulation that serves as a point of departure for a numerical solution.

A.1. Three-dimensional interfaces

Consider a collection of marker points in a three-dimensional interface, and label them using the two variables v^1 and v^2 that comprise a right-handed surface curvilinear coordinate system, as shown in figure 18(a). It is kinematically consistent to allow the marker points to move with the component of the velocity of the fluid normal to the interface, and with an arbitrary tangential component. The marker-point velocity is then

$$\mathbf{v} = (\mathbf{u} \cdot \mathbf{n}) \mathbf{n} + \mathbf{w}, \quad (\text{A } 1)$$

where \mathbf{w} is an arbitrary vector tangential to the interface. As a preliminary, we introduce the tangential component of the velocity of the fluid, also called the surface velocity, defined as

$$\mathbf{u}_s = \mathbf{n} \times \mathbf{u} \times \mathbf{n}, \quad (\text{A } 2)$$

where the subscript s stands for surface, and then the tangential vector field

$$\boldsymbol{\tau} = \mathbf{u}_s - \mathbf{w}. \quad (\text{A } 3)$$

When $\boldsymbol{\tau} = \mathbf{0}$, the marker points are point particles moving with the velocity of the fluid.

The rate of change of the surfactant concentration following a marker point is given by

$$\left(\frac{\partial \Gamma}{\partial t} \right)_{v^1, v^2} = -\boldsymbol{\tau} \cdot \nabla_s \Gamma - \Gamma \nabla_s \cdot \mathbf{u} + D_s \nabla_s^2 \Gamma, \quad (\text{A } 4)$$

where ∇_s and ∇_s^2 are the two-dimensional surface gradient and Laplacian operators

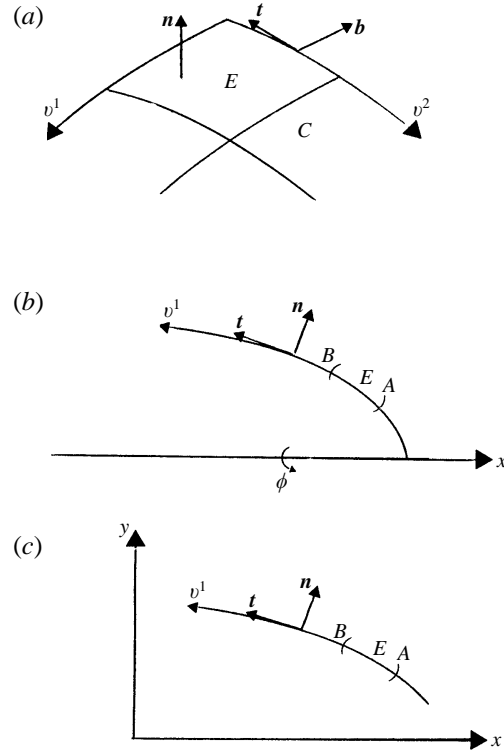


FIGURE 18. Curvilinear coordinates and a finite control-volume for a (a) three-dimensional, (b) axisymmetric, and (c) two-dimensional interface.

written with reference to a local Cartesian system with its axes tangential to the surface at the point where they are evaluated, and D_s is the surfactant diffusivity over the interface (e.g. Li & Pozrikidis 1997, equation (A 9)). We proceed by decomposing the interfacial velocity \mathbf{u} in the second term on the right-hand side of (A 4) into the normal and tangential components, writing $\mathbf{u} = (\mathbf{u} \cdot \mathbf{n}) \mathbf{n} + \mathbf{u}_s$, and obtain

$$\left(\frac{\partial \Gamma}{\partial t} \right)_{v^1, v^2} = -\boldsymbol{\tau} \cdot \nabla_s \Gamma - \Gamma \nabla_s \cdot \mathbf{u}_s - \Gamma \nabla_s \cdot (\mathbf{n}(\mathbf{u} \cdot \mathbf{n})) + D_s \nabla_s^2 \Gamma. \quad (\text{A } 5)$$

Combining the first two terms on the right-hand side with the help of (A 3), introducing the mean curvature of the interface κ_m and using the identity $\nabla_s \cdot \mathbf{n} = 2\kappa_m \mathbf{n}$ to restate the third term on the right-hand side, we arrive at the desired form

$$\left(\frac{\partial \Gamma}{\partial t} \right)_{v^1, v^2} = \mathbf{w} \cdot \nabla_s \Gamma - \nabla_s \cdot (\Gamma \mathbf{u}_s) - 2\Gamma \kappa_m \mathbf{u} \cdot \mathbf{n} + D_s \nabla_s^2 \Gamma. \quad (\text{A } 6)$$

When the marker points move with the velocity of the fluid normal to the interface, $\mathbf{w} = \mathbf{0}$, the first term on the right-hand side is absent.

To make (A 6) amenable to a finite-volume method of solution (e.g. Versteeg & Malalasekera 1996), we take the surface integral of both sides over an interfacial element E that is enclosed by the contour C , as shown in figure 18(a), and use the divergence theorem to obtain

$$\int_E \left(\frac{\partial \Gamma}{\partial t} \right)_{v^1, v^2} dS = \int_E \mathbf{w} \cdot \nabla_s \Gamma dS - \int_C \Gamma \mathbf{u}_s \cdot \mathbf{b} dl - 2 \int_E \Gamma \kappa_m \mathbf{u} \cdot \mathbf{n} dS + D_s \int_C \mathbf{b} \cdot \nabla_s \Gamma dl, \quad (\text{A } 7)$$

where dS and dl are, respectively, the differential surface area of E and the differential arclength along C . We have introduced the unit vector $\mathbf{b} = \mathbf{t} \times \mathbf{n}$, where \mathbf{t} is the unit vector that is tangential to C and points in the counterclockwise direction when the interface is observed from the outside, as depicted in figure 18(a). The implementation of the finite-volume method for solving (A 7) over the triangulated interface of a deforming drop is discussed by Yon & Pozrikidis (1998).

A.2. Axisymmetric interfaces

The surfactant concentration evolution equation for an axisymmetric interface follows readily by considering the trace of the interface in the (x, y) azimuthal plane denoted as C , labelling marker points distributed along C with the curvilinear coordinate v^1 , and identifying v^2 with the azimuthal angle θ , as shown in figure 18(b).

To develop the finite-volume formulation, we introduce the unit vector \mathbf{t} that is tangential to C and points in the direction of increasing v^1 , denote the corresponding arclength as l , and consider an interfacial element E with endpoints A and B , as shown in figure 18(b). Performing the integration in the azimuthal direction analytically, we find that equation (A 7) reduces to

$$\int_E \left(\frac{\partial \Gamma}{\partial t} \right)_{v^1} \sigma dl = \int_E \mathbf{w} \cdot \mathbf{t} \frac{\partial \Gamma}{\partial l} \sigma dl - (\Gamma \sigma \mathbf{u} \cdot \mathbf{t})_B + (\Gamma \sigma \mathbf{u} \cdot \mathbf{t})_A - \int_E \Gamma \kappa \mathbf{u} \cdot \mathbf{n} \sigma dl + D_s \left(\sigma \frac{\partial \Gamma}{\partial l} \right)_B - D_s \left(\sigma \frac{\partial \Gamma}{\partial l} \right)_A. \quad (\text{A } 8)$$

This equation is the starting point for the numerical procedure discussed in §2.

A.3. Two-dimensional interfaces

The differential form of the surfactant concentration evolution equation for a two-dimensional interface in the (x, y) -plane follows readily after a straightforward change in notation. In this case, the marker points are labelled using the single curvilinear coordinate v^1 , as shown in figure 18(c).

To implement the finite-volume formulation, we introduce the tangential unit vector along the interface \mathbf{t} , pointing in the direction of increasing v^1 , denote the corresponding arclength by l , and consider an interfacial element E with end points A and B , as shown in figure 18(c). The counterpart of (A 7) is

$$\int_E \left(\frac{\partial \Gamma}{\partial t} \right)_{v^1} dl = \int_E \mathbf{w} \cdot \mathbf{t} \frac{\partial \Gamma}{\partial l} dl - (\Gamma \mathbf{u} \cdot \mathbf{t})_B + (\Gamma \mathbf{u} \cdot \mathbf{t})_A - \int_E \Gamma \kappa \mathbf{u} \cdot \mathbf{n} dl + D_s \left(\frac{\partial \Gamma}{\partial l} \right)_B - D_s \left(\frac{\partial \Gamma}{\partial l} \right)_A, \quad (\text{A } 9)$$

where κ is the curvature of the trace of the interface in the (x, y) -plane. This equation is the starting point for the numerical procedure discussed in §2.

REFERENCES

- ANTANOVSKII, L. K. 1994*a* Quasi-steady deformation of a two-dimensional bubble placed within a potential viscous flow. *Meccanica* **29**, 27–42.
- ANTANOVSKII, L. K. 1994*b* Influence of surfactants on a creeping free-boundary flow induced by two counter-rotating horizontal thin cylinders. *Eur. J. Mech. B/Fluids* **13**, 73–92.
- ANTANOVSKII, L. K. 1994*c* A plane inviscid incompressible bubble placed within a creeping viscous flow: formation of a cusped bubble. *Eur. J. Mech. B/Fluids* **13**, 491–509.
- ANTANOVSKII, L. K. 1996 Formation of a pointed drop in Taylor's four-roller mill. *J. Fluid Mech.* **327**, 325–341.
- BETELÚ, S. 1997 Flujos de Stokes en el entorno de puntos singulares de superficies libres. Doctoral dissertation, Universidad Nacional del Centro de la Provincia Buenos Aires.
- BETELÚ, S., DIEZ, J. & GRATTON, R. 1997 Cusped ripples at the plane surface of a viscous liquid. Research manuscript.
- BRUIJN, R. A. DE 1993 Tip-streaming of drops in simple shear flow. *Chem. Engng Sci.* **48**, 277–284.
- BUCKMASTER, J. D. 1972 Pointed bubbles in slow viscous flow. *J. Fluid Mech.* **55**, 385–400.
- HOPPER, R. W. 1990 Plane Stokes flow driven by capillarity on a free surface. *J. Fluid Mech.* **213**, 349–375.
- JEONG, J.-T. & MOFFATT, H. K. 1992 Free-surface cusps associated with flow at low Reynolds number. *J. Fluid Mech.* **241**, 1–22.
- JOSEPH, D. D. 1992 Understanding cusped interfaces. *J. Non-Newtonian Fluid Mech.* **44**, 127–148.
- JOSEPH, D. D., NELSON, J., RENARDY, M. & RENARDY, Y. 1991 Two-dimensional cusped interfaces. *J. Fluid Mech.* **223**, 383–409.
- LI, X. & POZRIKIDIS, C. 1997 Effect of surfactants on drop deformation and on the rheology of dilute emulsions in Stokes flow. *J. Fluid Mech.* **341**, 165–194.
- MILLIKEN, W. J., STONE, H. A. & LEAL, L. G. 1993 The effect of surfactant on the transient motion of Newtonian drops. *Phys. Fluids A* **5**, 69–79.
- PAWAR, Y. & STEBE, K. J. 1996 Marangoni effects on drop deformation in an extensional flow: the role of surfactant physical chemistry. I. Insoluble surfactants. *Phys. Fluids A* **8**, 1738–1751.
- POZRIKIDIS, C. 1992 *Boundary Integral and Singularity Methods for Linearized Viscous Flow*. Cambridge University Press.
- POZRIKIDIS, C. 1997*a* *Introduction to Theoretical and Computational Fluid Dynamics*. Oxford University Press.
- POZRIKIDIS, C. 1997*b* Numerical studies of singularity formation at free surfaces and fluid interfaces in two-dimensional Stokes flow. *J. Fluid Mech.* **331**, 145–167.
- RICHARDSON, S. 1968 Two-dimensional bubbles in slow viscous flow. *J. Fluid Mech.* **33**, 475–493.
- RICHARDSON, S. 1997 Two-dimensional Stokes flow with time-dependent free boundaries driven by surface tension. *Eur. J. Appl. Maths* **8**, 311–329.
- SHERWOOD, J. D. 1984 Tip streaming from slender drops in a nonlinear extensional flow. *J. Fluid Mech.* **144**, 281–295.
- STONE, H. A. & LEAL, L. G. 1990 The effects of surfactants on drop deformation and breakup. *J. Fluid Mech.* **220**, 161–186.
- VERSTEEG, H. K. & MALALASEKERA, W. 1995 *An Introduction to Computational Fluid Dynamics; the Finite Volume Method*. Longman.
- YON, S. & POZRIKIDIS, C. 1998 A finite-volume/boundary-element method for flow past interfaces in the presence of surfactants, with application to shear flow past a viscous drop. Research manuscript.
- YOUNGREN, G. K. & ACRIVOS, A. 1976 On the shape of a gas bubble in a viscous extensional flow. *J. Fluid Mech.* **76**, 433–442.